

Process dependent thermoelectric transport properties of $\text{Ca}_3\text{Co}_4\text{O}_9$

Rapaka S C Bose, L Rangaraj, Abanti Nag*

Materials Science Division, CSIR-National Aerospace Laboratories, Bangalore 560017, India

*Corresponding author: Tel: (+91) 80 25086173; E-mail: abanti@nal.res.in

Received: 19 April 2017, Revised: 13 June 2017 and Accepted: 26 July 2017

DOI: 10.5185/amp.2017/804

www.vbripress.com/amp

Abstract

The *p*-type thermoelectric material $\text{Ca}_3\text{Co}_4\text{O}_9$ were synthesized by the sol-gel synthesis in the presence of complexing agent of citric acid and dispersant of polyethylene glycol 400, and followed by the uni-axial hot-pressing (HP) technique. Observation by X-ray diffraction revealed that the formation of phase pure sample on calcination at 1073 K for 4 h. Scanning electron microscopy indicated that the significant enhancement of the grain growth through HP technique. The density of the sintered pellets increased with an increase of applied pressure. The electrical resistivity was greatly reduced with an increase of the applied pressure, whereas the Seebeck coefficient was little increased with an increase of the applied pressure. As a result, the pellet treated by the HP technique under the condition of 1098 K, 25 MPa and 30 min showed a maximum power factor of about $498 \mu\text{Wm}^{-1}\text{K}^{-2}$ at 950K. Copyright © 2017 VBRI Press.

Keywords: Sol-gel processes, hot pressing, density, grain size.

Introduction

In recent times, the environment pollution and the energy crisis are the major critical global concerns. To overcome these problems, the extra energy sources for clean energy production other than fossil fuels are needed. Many alternative energy conversion technologies are being developed to produce clean energy. Among them, thermoelectric energy conversion technology has received renewed attention due to its direct energy conversion without any greenhouse gas emissions [1-7]. In order to estimate the thermoelectric materials efficiency, the following three physical properties are required: (1) low thermal conductivity (κ), which is necessary to introduce a large temperature gradient into both ends of the material, (2) low electrical resistivity (ρ), which is required to allow the electrical current in both the power generation and refrigeration mode and (3) large Seebeck coefficient (S), which is needed to generate high voltage per unit temperature gradient. Generally, the performance of the thermoelectric material is examined, in terms of the dimensionless figure of merit, $ZT = S^2 T \rho^{-1} \kappa^{-1}$ where Z and T are the figure of merit and the absolute temperature, respectively [7].

Commonly, the state-of-the art thermoelectric devices are based on Bi-Te, Bi-Se, Se-Ge and Pb-Te alloys because of high thermoelectric energy conversion efficiency. Unfortunately, these compounds are found to have limited practical uses at high temperature ($T \sim 1000$ K) because they can easily decompose, vaporize, melt and get oxidized in air at high temperatures. Moreover, employing these high expensive and heavy metals should

be given a second thought, as they are usually toxic, scarcely available in natural resources and hazardous to the environment. In the light of the above-mentioned problems, metal oxides are found to be more suitable for high temperature thermoelectric applications due to their chemical and structural stabilities, oxidation resistance, ease of manufacturing, lightweight and low cost [8-12]. The thermoelectric metal oxides are categorized based on the crystal structure in four different classes as: (i) layered cobalt oxides (Na_xCoO_2 , $\text{Ca}_3\text{Co}_4\text{O}_9$ and $\text{Bi}_2\text{Sr}_2\text{Co}_2\text{O}_y$), (ii) perovskite based oxides (SrTiO_3 and CaMnO_3), (iii) wide band-gap semiconductor oxides (ZnO , SnO_2 and In_2O_3) and (iv) layered oxychalcogenides (BiCuSeO).

To improve the thermoelectric performance, it is required to prepare low grain size $\text{Ca}_3\text{Co}_4\text{O}_9$ ceramics followed by development of high density polycrystalline samples. To achieve the high dense samples, various methods are proposed such as hot pressing (HP) [13, 14], hydrothermal hot-pressing [15, 16], cold high-pressure fabrication [17], thermo forging [18] and spark plasma sintering [19, 20] (Table 1). Among the above-mentioned techniques, spark plasma sintering and HP techniques are the best methods to improve thermoelectric performance. But the spark plasma sintering technique produces high dense materials with a reduced orientation degree [19] and a lack of homogeneity in the microstructure [21, 22], whereas the HP technique is expected to be more effective for the formation of high density material with a good orientation degree. In this work, highly dense and structurally oriented thicker $\text{Ca}_3\text{Co}_4\text{O}_9$ samples are fabricated by uni-axial HP technique in combination with the sol-gel method in the presence of a complexing agent

Table 1. The comparison of the reported work with the conventional techniques reported in the literature for synthesis of $\text{Ca}_3\text{Co}_4\text{O}_9$

Synthesis Methodology	Advantages	Disadvantages	References
Solid-state methodology	Very fast and economic process	Low density of materials	17
Hydrothermal hot-pressing	Higher density material	Poor yield	15, 16
Cold high-pressure fabrication	Very fast process equivalent to solid-state methodology	Low density of materials	17
Thermo forging	High density	Lower homogeneity	18
Spark-plasma sintering	High density and lower particle size	Lack of homogeneity and lower orientational degree	19, 20, 21, 22
Hot-press sintering	High density	Higher particle size	13,14
Sol-gel synthesis followed by Hot-press sintering	High density and good orientational degree	Slightly higher particle size than spark-plasma sintering	This paper

of citric acid and dispersant of polyethylene glycol 400. In order to further understand the effect of the HP technique on the physical properties, especially the thermoelectric properties of the $\text{Ca}_3\text{Co}_4\text{O}_9$, the correlation between the microstructure and density with the thermoelectric properties are investigated in this paper.

Experimental

Chemicals details

The polycrystalline powder of $\text{Ca}_3\text{Co}_4\text{O}_9$ was prepared by wet chemical sol-gel method in the presence of citric acid as complexing agent and polyethylene glycol as dispersant. High purity precursors CaCO_3 (Alfa Aesar & 99.99%), $\text{Co}(\text{NO}_3)_2 \cdot 6\text{H}_2\text{O}$ (Alfa Aesar & 99.999%), citric acid (Alfa Aesar & 99.5%) and polyethylene glycol 400 (Alfa Aesar) (PEG) were used.

Material synthesis

Proper stoichiometric amounts of metal nitrates were dissolved in distilled water with constant stirring, and then citric acid (1:2 of metal ion to citric acid) was added to make a solution complex (sol). After addition of 2% (volume ratio) PEG, the resulting solution was stirred on a magnetic stirrer at 353K in order to obtain the gel. The gel was dried initially at 423 K for 2 h and further heat treated in air at temperature 1073 K for 4 h with intermediate grindings in order to remove the remaining organics and decompose of the nitrates in the gel. The obtained phase pure powders were processed for sintering using the following methods: (i) Solid-state sintering (SS), (ii) Hot-press sintering (HP) and (iii) Solid-state sintering followed by hot-press sintering (SSHP). The disc pellet was pre-sintered at 1073 K for 30 min before hot-pressing in SSHP method, whereas the phase-pure powder was hot-pressed directly in HP method. The experimental conditions for these processes were listed in **Table 2**.

Table 2. The experimental conditions of different methods.

Methodology	Experimental Conditions		
	Temperature (K)	Pressure (MPa)	Time (min)
Solid-state sintering (SS)	1098	0	300
Hot-press sintering (HP)	1098	15 & 25	30
Solid-state sintering followed by hot-press sintering (SSHP)	1098	25	30

Characterizations

The phase identification of the samples obtained was observed by X-ray diffraction on a Bruker D8 Advanced X-ray diffractometer (Ni filtered Cu K_α radiation). The morphology of the processed $\text{Ca}_3\text{Co}_4\text{O}_9$ ceramics was examined using scanning electron microscopy on a LEO Electron microscopy from Oxford Instruments. The XRD and SEM measurements were performed at room temperature on the polished surface of the disc pellets. The density values were determined from the mass and volume of the disc pellets and confirmed through Archimedes method. The relative percent density of these samples was computed by comparing the sample density to the theoretical density reported for the $\text{Ca}_3\text{Co}_4\text{O}_9$ phase. The temperature dependence of the electrical resistivity ($\rho(T)$) and Seebeck coefficient ($S(T)$) were measured on a bar-shaped sample ($2.5 \times 3.5 \times 12 \text{ mm}^3$) in the 300-950 K range at ambient pressure using an in-house resistivity and thermopower set-up.

Results and discussion

All the powder XRD patterns of the $\text{Ca}_3\text{Co}_4\text{O}_9$ powder, prepared at different ratios of citric acid and PEG combinations are identical to the previously reported data for the $\text{Ca}_3\text{Co}_4\text{O}_9$ structure [23, 24] (**Fig. S1**), indicating the formation of single phase compounds. No observable traces of impurity phases are detected. From this XRD data, the crystalline sizes of the samples are calculated using the Scherrer's equation given as follows:

$$D = \frac{K\lambda}{\beta \cos\theta} \quad (1)$$

where, D is the crystallite size, K is the shape factor, which usually takes a value about 0.94, λ is the X-ray wavelength (0.15418 nm), β is the full width half-maximum of the diffraction peak at θ , which is the diffraction angle. The high intense peaks of (002), (003), (004) and (201) planes are selected to calculate the average crystallite size. The average crystallite sizes of $\text{Ca}_3\text{Co}_4\text{O}_9$ synthesized varying the concentration of citric acid and PEG are tabulated in **Table S1**. The above results indicate that the powder obtained by a sol-gel process in the presence of 1:2 ratio of metal ion to citric acid and 2% (volume ratio) of PEG has the lowest crystallite sizes.

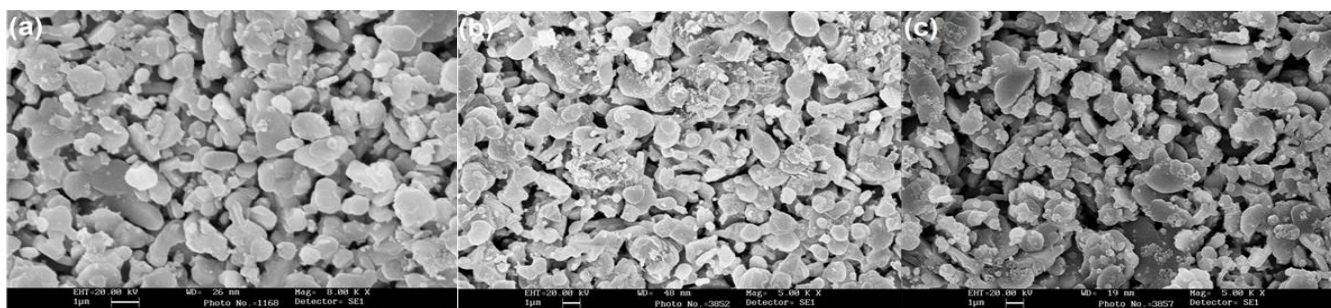


Fig. 1. SEM micrographs showing cross-section of the $\text{Ca}_3\text{Co}_4\text{O}_9$ pellets (a) 1:1 of metal ion to citric acid, (b) 1:2 of metal ion to citric acid, and (c) 1:2 of metal ion to citric acid and 2% (volume ratio) PEG.

Fig. 1 shows the SEM micrographs of $\text{Ca}_3\text{Co}_4\text{O}_9$ prepared by the sol-gel method with different concentration of citric acid and PEG. The SEM micrographs of $\text{Ca}_3\text{Co}_4\text{O}_9$ prepared by the sol-gel method with 1:1 of metal ion to citric acid (**Fig. 1 (a)**) and with 1:2 of metal ion to citric acid (**Fig. 1 (b)**) show strong grain agglomeration and large grain sizes whereas the SEM micrograph of $\text{Ca}_3\text{Co}_4\text{O}_9$ prepared by the sol-gel method with 1:2 of metal ion to citric acid in the presence of 2% (volume) of PEG (**Fig. 1 (c)**) shows less grain agglomeration and low grain sizes. The average grain sizes of $\text{Ca}_3\text{Co}_4\text{O}_9$ prepared by the sol-gel method with different concentration of citric acid and PEG are tabulated in **Table S1**. The above results indicate that the powder prepared by sol-gel process with 1:2 of metal ion to citric acid in the presence of 2% (volume ratio) of PEG has the lowest grain sizes which are in good agreement with the XRD results.

Generally, the thermoelectric properties depend on the grain sizes [23, 25] and chemical homogeneity. Therefore, to improve the thermoelectric properties, low grain sizes and high chemical homogeneity are important phenomena to achieve. Although solid state synthesis is very simple method to synthesize $\text{Ca}_3\text{Co}_4\text{O}_9$ ceramics, this process possesses several serious drawbacks, such as large grain sizes and limited degree of chemical homogeneity [26]. But sol-gel synthesis method is one of the best synthesis method to produce low grain size and high homogeneous powders at low temperature. As observed from XRD and SEM analyses, grain size of $\text{Ca}_3\text{Co}_4\text{O}_9$ depends on the concentration of the citric acid and PEG. The grain sizes of the powders decrease with increasing the concentration of citric acid [27, 23] and PEG [23, 24]. When the dispersant PEG is added to the sol, the dispersant reduces the surface tension of sol solution significantly and keeps the sol particles separated in the solution due to polymeric dispersant of long chain molecule [28, 29]. This indicates that the PEG reduces the agglomeration of grains, thereby leading to decrease the grain sizes correspondingly. On the other hand, without PEG, the primary sol particles from this solution are unstable against agglomeration since the surface tension is sufficiently high. Therefore, the final $\text{Ca}_3\text{Co}_4\text{O}_9$ grains prepared without PEG appear to have poor dispersibility whereas the $\text{Ca}_3\text{Co}_4\text{O}_9$ grains prepared with PEG appear to have high dispersibility. However, the density and degree of grain orientation of

ceramics may be low when it is prepared by the sol-gel method. It is considered that the homogeneous phase without agglomeration and low grain size grains can provide increase of the Seebeck coefficient [30] and may cause the little increase of electrical resistivity [27] thereby leading to improved thermoelectric energy conversion efficiency. However, the grain sizes may produce different effects for different materials. Therefore, $\text{Ca}_3\text{Co}_4\text{O}_9$ phase pure powder obtained by a sol-gel process in the presence of 1:2 of metal ion to citric acid and 2% (volume ratio) of PEG is used for further processes.

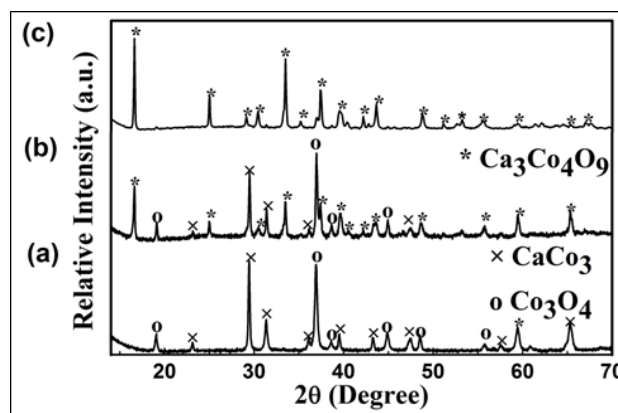


Fig. 2. XRD pattern showing phase formation of $\text{Ca}_3\text{Co}_4\text{O}_9$; (a) 873 K/12 h, (b) 973 K/12 h and (c) 1073 K/4 h.

According to the binary phase diagram of CaO and CoO (**Fig. S2**), single phase $\text{Ca}_3\text{Co}_4\text{O}_9$ appears below 1199 K (926 °C) and decompose to another phase at higher temperatures [31]. To check the formation of phase pure $\text{Ca}_3\text{Co}_4\text{O}_9$ at lower calcination temperature, the crushed gel is calcined at temperatures between 873 K and 1073 K. **Fig.2** shows the XRD patterns of the $\text{Ca}_3\text{Co}_4\text{O}_9$ phase evaluation at different calcination temperatures. The formation of $\text{Ca}_3\text{Co}_4\text{O}_9$ as a single phase is temperature dependent. After calcining at 873 K for 12 h, CaCO_3 (JCPDS card no. 85-1108) and Co_3O_4 (JCPDS card no. 80-1545) phases are detected. Increasing the calcinations temperatures to 973 K for 12 h, $\text{Ca}_3\text{Co}_4\text{O}_9$ phase starts forming, with a small amount of residual CaCO_3 and Co_3O_4 . Further increase of the calcinations temperature to 1073 K for 4 h, pure phase of $\text{Ca}_3\text{Co}_4\text{O}_9$ (JCPDS card no. 21-0139) is obtained. The above result

indicates that the phase pure $\text{Ca}_3\text{Co}_4\text{O}_9$ is obtained at 1073 K temperature [27, 23, 24].

The calculated density values are listed in Table 3. The highest density values are obtained for both SSHP at 25 MPa (4.35 g/cm^3 & ~95%) and HP at 25 MPa (4.47 g/cm^3 & ~98%) samples. This result indicates that the density increases with increasing applied pressure. High bulk density is needed to improve the thermoelectric properties. This result concludes that the HP technique is useful to make the dense thicker samples for the practical applications.

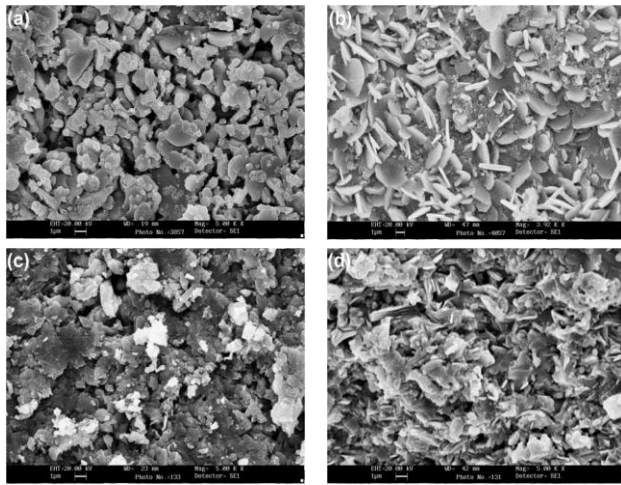


Fig. 3. SEM micrographs showing cross-sections of the $\text{Ca}_3\text{Co}_4\text{O}_9$ pellets (a) Solid-state sintering (SS), (b) Solid-state sintering followed by hot-press sintering (SSHP) at 25 MPa, (c) Hot-press sintering (HP) at 15 MPa, and (d) Hot-press sintering (HP) at 25 MPa samples.

Fig. 3 shows the SEM microstructure of surface of the $\text{Ca}_3\text{Co}_4\text{O}_9$ samples are processed by different sintering methods. In the case of SS micrograph (**Fig. 3 (a)**), round shaped, loosely assembled grains are observed with no preferred orientation. In the case of the SSHP at 25 MPa pressure, micrograph (**Fig. 3 (b)**) of plate-like, closely packed, larger, more homogenous and oriented grains are observed. In the case of HP at 15 and 25 MPa pressures, micrographs (**Fig. 3 (c) and (d)**) of sheet-like, closely packed, larger, more homogenous and oriented grains are observed. The average grain sizes of $\text{Ca}_3\text{Co}_4\text{O}_9$ processed by different sintering methods are listed in Table 3. This result shows that the HP technique increases the grain growth thereby contributing to improve the grain contacts

with increasing pressure. It is relevant to note here that the microstructure and density achieved in the hot-press samples exhibit much better thermoelectric characteristics sought for reducing the electrical resistivity compared to the SS sample.

Fig.S3 shows the XRD patterns of the $\text{Ca}_3\text{Co}_4\text{O}_9$ pellets processed by SS, HP and SSHP methods. It indicates that the HP technique does not change the crystal structure of the system. All X-ray peaks are shown in **Fig. S3** are well indexed. In addition, X-ray diffraction patterns of $\text{Ca}_3\text{Co}_4\text{O}_9$ ceramics reveal high intense peaks indexed as (00l), whereas the other diffraction peaks are relatively weaker than (00l). This implies that the crystal grains grow along the c-axis to form an oriented structure [13]. The structure of $\text{Ca}_3\text{Co}_4\text{O}_9$ is composed of stacks of CdI₂-type CoO_2 layer (subsystem 1) alternating with rock-salt-type Ca_2CoO_3 layer (subsystem 2) along the c-axis and can be denoted as $[\text{Ca}_2\text{CoO}_3]_{\text{RS}}[\text{CoO}_2]_{1.62}$ [17, 32, 33]. The misfit relation between the two subsystems leads to an incommensurate structure with the subsystems sharing the same a, c and β parameters but different b lattice parameters ($b_1/b_2 = 1.62$) [34-36]. **Fig. S4** shows the crystal structure of layered cobalt oxide $\text{Ca}_3\text{Co}_4\text{O}_9$ along the c-axis.

In order to check the effect of hot-press on the oriented structure quantitatively, the Lotgering factor (*F*) is used to evaluate the degree of crystal grain orientation, in which the value of *F* is calculated by using the XRD peak intensity [37]. The Lotgering factor is usually defined as

$$F = (P - P_o) / (I - P_o) \quad (2)$$

where, $P = \sum I(00l) / \sum I(hkl)$ and $P_o = \sum I_o(00l) / \sum I_o(hkl)$; P_o can be calculated from the peak data of the JCPDS card (JCPDS card no. 21-0139). The *F* value is zero ($F = 0$) for a crystallographic isotropic (randomly oriented) sample i.e. the value of *P* is P_o ; and *F* value is one ($F = 1$) for a completely oriented sample along c-axis direction. The calculated *F* values are listed in Table 3. It indicates that the *F* value increases monotonously with increasing applied pressure, implying that the crystal grains tend to orient along the c-axis i.e. the direction of applied pressure. The fact of the orientation of the crystal grains orient along the applied pressure indicates that the c-axis is the easy oriented axis for the $\text{Ca}_3\text{Co}_4\text{O}_9$ system.

Table 3. Structural and thermoelectric properties of $\text{Ca}_3\text{Co}_4\text{O}_9$ ceramics at different applied pressure.

$\text{Ca}_3\text{Co}_4\text{O}_9$	Solid-state sintered (SS)	Hot-press sintering (HP) at 15 MPa	Hot-press sintering (HP) at 25 MPa	Solid-state sintering followed by hot-press sintering (SSHP) at 25 MPa
Grain size (μm)	0.2-0.8	0.6-3.0	1.0-2.8	1.4-3.8
Density (g/cc)	2.65	3.96	4.47	4.35
Relative density (%)	58	86	98	95
<i>F</i>	0.30	0.53	0.77	0.78
$\rho_{300\text{K}}$ (m Ω .cm)	33	28	11	14
$\rho_{950\text{K}}$ (m Ω .cm)	28	9	6	7
$S_{300\text{K}}$ (μVK^{-1})	84	96	115	106
$S_{950\text{K}}$ (μVK^{-1})	165	158	181	180
$P_{950\text{K}}$ ($\mu\text{Wm}^{-1}\text{K}^{-2}$)	120	244	498	474

This result shows that a much higher degree of *c*-axis preferred orientation is noted in the SSHP and HP at 25 MPa samples than in other samples. It is relevant to note here that the hot-press technique is explored to process the $\text{Ca}_3\text{Co}_4\text{O}_9$ materials in an effort to increase the orientation and density thereby leading to ease the movement of charge carriers and subsequently, reduce the electrical resistivity.

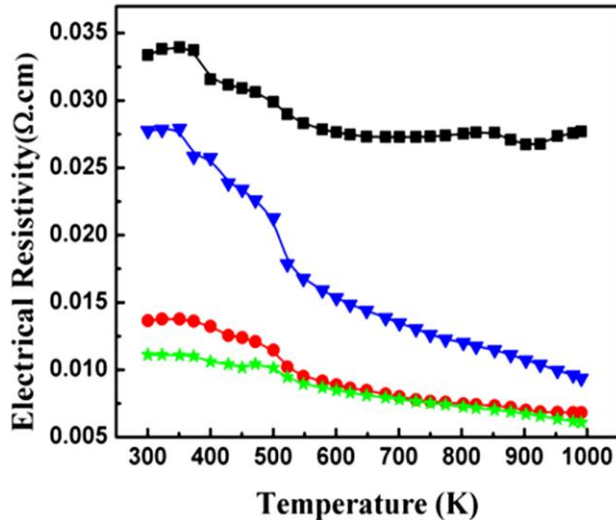


Fig. 4. Electrical resistivity as a function of temperature for (■) Solid-state sintering (SS), (▼) Hot-press sintering (HP) at 15 MPa, (●) Solid-state sintering followed by hot-press sintering (SSHP) at 25 MPa, and (★) Hot-press sintering (HP) at 25 MPa samples.

Fig. 4 shows the temperature dependence of the electrical resistivity ($\rho(T)$) measured in the 300-950 K range. The lowest electrical resistivity values are obtained for both SSHP at 25 MPa (7 mΩ.cm) and HP at 25 MPa (6 mΩ.cm) samples at 950 K. The room temperature electrical resistivity values of HP at 25 MPa and SSHP at 25 MPa are consistent with the values reported for $\text{Ca}_3\text{Co}_4\text{O}_9$ single crystals by *Masset et al.* (12 mΩ.cm) [32] and for the hot-press processed $\text{Ca}_3\text{Co}_4\text{O}_9$ polycrystalline samples by *Xu et al.* (10.5 mΩ.cm) [38]. The electrical resistivity values at 950 K of both SSHP at 25 MPa and HP at 25 MPa samples are in good agreement with that reported for the hot-press processed $\text{Ca}_3\text{Co}_4\text{O}_9$ polycrystalline samples by *Kenfai et al.* [13].

The resistivity curves show a transition around $T^* = 400$ K, which is attributed to be associated with a Co spin transition [39, 40] or structural change [41]. It shows that the resistivity curves for all samples show a metallic-like behavior ($d\rho/dT > 0$) below T^* and semiconducting-like transport behavior ($d\rho/dT < 0$) above T^* . That is to say, there exists a M-I transition in the resistivity curves for all samples at T^* . The dropping of electrical resistivity near T^* contributes greatly to power factor enhancement at high temperature because the Seebeck coefficient increases monotonically from room temperature to 950 K. Hence the resistivity anomaly may impact the high temperature thermoelectric properties.

A marked anisotropy in the electrical resistivity values evidences by a large gap between solid-state sintered and hot-pressed electrical resistivity values. Such anisotropy can be derived from: (i) grain sizes and (ii) density/porosity.

Generally, the electrical resistivity ρ is expressed by,

$$\rho = \frac{1}{ne\mu} \quad (3)$$

where, n is the number of charge carriers, e is the electron charge (1.6021×10^{-19} C) and μ is the charge carrier mobility. From equation 3, the electrical resistivity of thermoelectric materials is mainly determined by the carrier concentration (ne) and the carrier mobility.

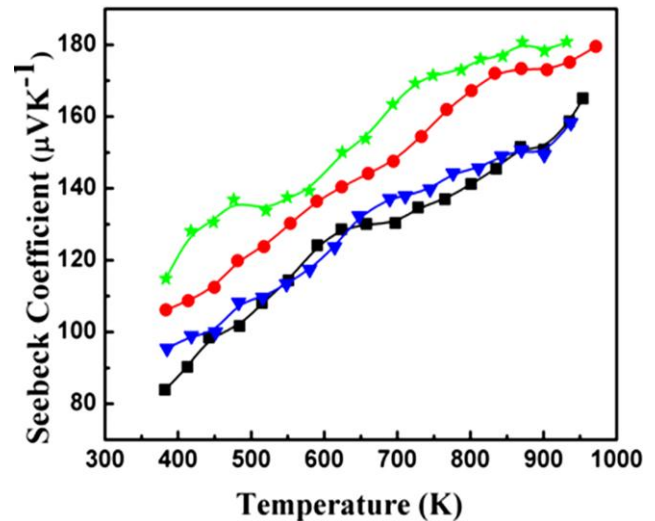


Fig. 5. Seebeck coefficient as a function of temperature for (■) Solid-state sintering (SS), (▼) Hot-press sintering (HP) at 15 MPa, (●) Solid-state sintering followed by hot-press sintering (SSHP) at 25 MPa, and (★) Hot-press sintering (HP) at 25 MPa samples.

Grain sizes and porosity play an important role to evaluate the electrical resistivity values of the samples. In the case of solid-state sintering sample, the grains are smaller and porous caused for low grain contacts at grain boundaries. In the case of hot-pressed samples, the grains are large and closely packed thereby leading to improve the grain contacts at grain boundaries. Moreover, smaller grains are having large number of grain boundaries thereby leading to increase the scattering of charge carriers, whereas large grains are having less number of grain boundaries thereby contributing to decrease the scattering of charge carriers. The resistivity of the solid-state sintering sample is higher than that of hot-pressed samples due to the high porosity and high charge scattering. Thus, the carrier mobility of charge carriers might increase with increasing grain sizes and density. Therefore, the resistivity values decrease with increasing grain sizes and density.

Fig. 5 shows the temperature dependence of the Seebeck coefficient ($S(T)$) measured at temperature range from 300 K to 950 K on the same bar-shaped samples. The Seebeck coefficient of all samples shows a positive

value in the whole measured temperature range, indicating *p*-type conducting transport behavior i.e. majority carriers are holes. Further the increase of *S* value with temperature confirms the hole as a charge carrier. The highest Seebeck coefficient values are obtained for both SSHP at 25 MPa (180 μVK^{-1}) and HP at 25 MPa (181 μVK^{-1}) samples at 950 K. The Seebeck coefficient values of all samples at 950 K are in good agreement with the values reported in literature [13]. Most reported Seebeck coefficients are in the range of 175-185 $\mu\text{V/K}$ at 1000 K irrespective of the density of bulk $\text{Ca}_3\text{Co}_4\text{O}_9$ samples [42, 15]. The thermopower of $\text{Ca}_3\text{Co}_4\text{O}_9$ can be estimated using Heikes formula [43]

$$S = -\frac{k_B}{e} \ln \left[\frac{g_3}{g_4} \left(\frac{x}{1-x} \right) \right] \quad (4)$$

where, g_3 and g_4 are the spin-orbital degeneracy for Co^{3+} and Co^{4+} ions in the CoO_2 layers, respectively, x is the Co^{4+} concentration in these layers, and k_B is the Boltzmann constant. Considering $g_3/g_4 = 1/6$ [44], the theoretical *S* value is estimated to $S_{\text{theo}} = -155 \mu\text{VK}^{-1}$, which is in good agreement with experimental values.

As compared with the SS sample, the applied pressure in the HP samples does not change the shape of the *S*(*T*) curve on the whole but changes the values of *S* considerably. The Seebeck coefficient values of all the samples only differ by 7-15 μVK^{-1} . The value of the Seebeck coefficient varies slightly when increasing the applied pressure, which indicates that the density and microstructure had little influence on the Seebeck coefficient values [45]. As previously reported in literature, when the size of the grains decreases, the Seebeck coefficient should increase due to the energy filtering effect. However, in our study, we observed that the Seebeck coefficient is increased with increasing grain sizes as reported [23]. The reason could be explained as follows. Due to the high porosity in sample, which leads to increase the density of the scattering region, in turn leads to scatter carriers more by porosity. That is to say, the contribution of charge carrier to enhance the Seebeck coefficient decreases. Therefore, it can be concluded that while smaller grain size has a positive effect on the Seebeck coefficient, porosity has negative effect [23]. The porosity is decreased with increasing applied pressure, confirmed from SEM micrographs. It indicates that the low porous sample might show little high Seebeck coefficient values.

Fig.6 shows the temperature dependence of the power factor, which is calculated from the electrical resistivity and Seebeck coefficient values. The values of *P* at 950 K, $P_{950\text{K}}$, reaches 498 $\mu\text{Wm}^{-1}\text{K}^{-2}$, and 474 $\mu\text{Wm}^{-1}\text{K}^{-2}$ for the HP at 25 MPa and SSHP at 25 MPa samples, respectively. The HP at 25 MPa sample shows the little large power factor than the SSHP at 25 MPa sample. This is clearly linked to the little low resistivity and little high Seebeck coefficient values obtained for the HP at 25 MPa sample. The power factor is about four times larger than that of the solid-state sintered sample (Table 3).

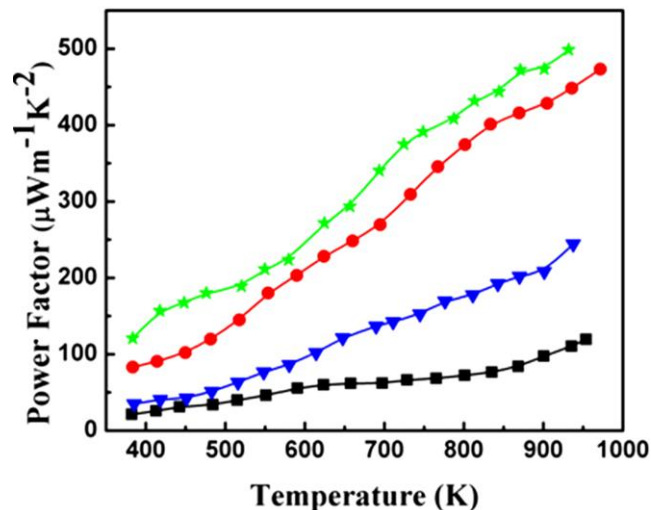


Fig. 6. Power factor as a function of temperature for (■) Solid-state sintering (SS), (▼) Hot-press sintering (HP) at 15 MPa, (●) Solid-state sintering followed by hot-press sintering (SSHP) at 25 MPa and (★) Hot-press sintering (HP) at 25 MPa samples.

Conclusion

We synthesize $\text{Ca}_3\text{Co}_4\text{O}_9$ ceramics by the citrate sol-gel in the presence of PEG followed by HP sintering and examined their microstructure and thermoelectric properties. This sol-gel method is useful for preparing a fine powder, and the HP technique is a method by which dense and oriented $\text{Ca}_3\text{Co}_4\text{O}_9$ can be produced from powders at 1098 K temperature at 25 MPa pressure. With an increase of the applied pressure during the HP technique, the electrical resistivity of the samples decreases but a little difference is present between the values of Seebeck coefficient of the samples. The electrical resistivity of the samples by this synthesis method and hot-press technique is smaller than that of the sample by the solid-state sintering, and the power factor of the former is larger than that of the later.

Acknowledgements

We thank Dr. Anjana Jain for powder XRD data and Ms. Kalavati for SEM micrographs (both from Materials Science Division of NAL). Financial support by Council of Scientific and Industrial Research and Science and Engineering Research Board, Department of Science and Technology, Government of India (SERB/F/4679/2013-14) are gratefully acknowledged.

Author's contributions

All the authors have contributed equally. Authors have no competing financial interests.

Supporting information

Supporting informations are available from VBRI Press.

References

- DiSalvo, F. J.; *Science*, **1999**, 285, 703. DOI:10.1126/science.285.5428.703
- Snyder, G.J.; Toberer, E. S.; *Nature Mater.* **2008**, 7, 105. DOI:10.1038/nmat2090
- Bell, L. E.; *Science*, **2008**, 321, 1457. DOI:10.1126/science.1158899.

4. Tritt, T. M.; Recent Trends in Thermoelectric Materials Research I & II, in Semiconductors and Semimetals, Academy Press, USA, **2001**.
5. Rowe, D. M.; Thermoelectrics Handbook: Micro to Nano, CRC Press, Taylor & Francis Group, USA, **2006**.
6. Winder, E.J.; Ellis, A.B.; Lisenksy, G.C.; *J. Chem. Educ.***1996**, *73*, 940.
DOI: [10.1021/ed073p940](https://doi.org/10.1021/ed073p940)
7. Nolas, G. S.; Sharp, J.; Goldsmid, H. J.; Thermoelectrics, Basic Principles and New Materials Developments, Springer-Verlag Berlin Heidelberg, Germany, **2001**.
8. Ohta, H.; Suglura, K.; Koumoto, K.; *Inorg. Chem.***2008**, *47*, 8429.
DOI: [10.1021/ic800644x](https://doi.org/10.1021/ic800644x).
9. Ohtaki, M.; *Program Novel Carbon Resources Sciences*.**2010**, *3*, 8.
10. Koumoto, K.; Wang, Y. F.; Zhang, R. Z.; Kosuga, A.; Funahashi, R.; *Annu. Rev. Mater. Res.***2010**, *40*, 363.
DOI: [10.1146/annurev-matsci-070909-104521](https://doi.org/10.1146/annurev-matsci-070909-104521)
11. Nag, A.; Shubha, V.; *J. Electron. Mater.***2014**, *43*, 962.
DOI: [10.1007/s11664-014-3024-6](https://doi.org/10.1007/s11664-014-3024-6)
12. Maignan, A.; Hebert, S.; Pi, L.; Pelloquin, D.; Martin, C.; Michel, C.; Hervieu, M.; Raveau, B.; *Cryst. Eng.***2002**, *5*, 365.
DOI: [10.1016/S1463-0184\(02\)00048-5](https://doi.org/10.1016/S1463-0184(02)00048-5)
13. Kenfaui, D.; Chateigner, D.; Gomina, M.; Noudem, J. G.; *Int. J. Appl. Ceram. Technol.***2011**, *8*, 214.
DOI: [10.1111/j.1744-7402.2009.02431.x](https://doi.org/10.1111/j.1744-7402.2009.02431.x)
14. Prasoetsopha, N.; Pinitsoontom, S.; Amomkitbamrung, V.; *Electron. Mater. Lett.***2012**, *8*, 305.
DOI: [10.1007/s13391-012-1088-0](https://doi.org/10.1007/s13391-012-1088-0)
15. Katsuyama, S.; Takiguchi, Y.; Ito, M.; *Mater. Trans.***2007**, *48*, 2073.
DOI: [10.2320/matertrans-E-MRA2007805](https://doi.org/10.2320/matertrans-E-MRA2007805)
16. Katsuyama, S.; Takiguchi, Y.; Ito, M.; *J. Mater. Sci.***2008**, *43*, 3553.
DOI: [10.1007/s10853-008-2561-x](https://doi.org/10.1007/s10853-008-2561-x)
17. Wang, Y.; Sui, Y.; Wang, X.; Su, W.; Liu, X.; *Appl. Phys.***2010**, *107*, 033708.
DOI: [10.1063/1.3291125](https://doi.org/10.1063/1.3291125)
18. Prevel, M.; Lemonnier, S.; Klein, Y.; Hebert, S.; Chateigner, D.; Ouladdiaf, B.; Noudem, J. G.; *J. Appl. Phys.***2005**, *98*, 09370.
DOI: [10.1063/1.2120892](https://doi.org/10.1063/1.2120892)
19. Liu, Y.; Lin, Y.; Shi, Z.; C. Nan, W.; Shen, Z.; *J. Am. Ceram. Soc.***2005**, *88*, 1337.
DOI: [10.1111/j.1551-2916.2005.00284.x](https://doi.org/10.1111/j.1551-2916.2005.00284.x)
20. Lim, C.H.; Seo, W.S.; Lee, S.; Soo Lim, Y.; Kim, J. Y.; Park, H. H.; Choi, S. M.; Lee, K. H.; Park, K.; *J. Korean Phys. Soc.***2015**, *66*, 794.
DOI: [10.3938/jkps.66.794](https://doi.org/10.3938/jkps.66.794)
21. Tokita, M.; *Mater. Sci. Forum***1999**, *308*, 83.
DOI: [10.4028/www.scientific.net/MSF.308-311.83](https://doi.org/10.4028/www.scientific.net/MSF.308-311.83)
22. Orru, R.; Licheri, R.; Locci, A. M.; Cincotti, A.; Cao, G.; *Mater. Sci. Eng.***2009**, *R63*, 127.
DOI: [10.1016/j.mser.2008.09.003](https://doi.org/10.1016/j.mser.2008.09.003)
23. Gunes, M.; Ozenbas, M.; *J. Alloys Compd.***2015**, *626*, 360.
DOI: [10.1016/j.jallcom.2014.12.004](https://doi.org/10.1016/j.jallcom.2014.12.004)
24. Zhang, Y. F.; Zhang, J. X.; Lu, Q. M.; Zhang, Q. Y.; *Mater. Lett.***2006**, *60*, 2443.
DOI: [10.1016/j.matlet.2006.01.013](https://doi.org/10.1016/j.matlet.2006.01.013)
25. Zhang, R.; Wang, C.; Li, J.; Koumoto, K.; *J. Am. Ceram. Soc.***2010**, *93*, 1677.
DOI: [10.1111/j.1551-2916.2010.03619.x](https://doi.org/10.1111/j.1551-2916.2010.03619.x)
26. Horii, S.; Matsubara, I.; Sano, M.; Fujie, K.; Suzuki, M.; Funahashi, R.; Shikano, M.; Shin, W.; Muarayama, N.; Shimoyama, J.; Kishio, K.; *Jpn. J. Appl. Phys.***2003**, *42*, 7018.
DOI: [10.1143/JJAP.42.7018](https://doi.org/10.1143/JJAP.42.7018)
27. Qi, X.; Zeng, L.; Wang, H.; Liu, P.; Liu, Y.; *J. Wuhan Uni. Tech. Mat. Sci. Ed.***2010**, *25*, 287.
DOI: [10.1007/s11595-010-2287-x](https://doi.org/10.1007/s11595-010-2287-x)
28. Yang, J.; Lian, J.; Dong, Q.; Guan, Q.; Chen, J.; Guo, Z.; *Mater. Lett.***2003**, *57*, 2792.
DOI: [10.1016/S0167-577X\(02\)01376-9](https://doi.org/10.1016/S0167-577X(02)01376-9)
29. Ferri, J. K.; Stebe, K. J.; *Adv. Colloid Interface Sci.***2000**, *85*, 61.
DOI: [10.1016/S0001-8686\(99\)00027-5](https://doi.org/10.1016/S0001-8686(99)00027-5)
30. Zhang, R.; Koumoto, K.; *J. Electron. Mater.* **2013**, *42*, 1568.
DOI: [10.1007/s11664-012-2324-y](https://doi.org/10.1007/s11664-012-2324-y)
31. Sedmidubsky, D.; Jakes, V.; Jankovsky, O.; Leitner, J.; Sofer, Z.; Hejtmanek, J.; *J. Solid state Chem.***2012**, *194*, 199.
DOI: [10.1016/j.jssc.2012.05.014](https://doi.org/10.1016/j.jssc.2012.05.014)
32. Masset, A. C.; Michel, C.; Maignan, A.; Hervieu, M.; Toulemonde, O.; Studer, F.; Raveau, B.; Hejtmanek, J.; *Phys. Rev. B.***2000**, *62*, 166.
DOI: [10.1103/PhysRevB.62.166](https://doi.org/10.1103/PhysRevB.62.166)
33. Kanno, T.; Yotsuhashi, S.; Adachi, H.; *Appl. Phys. Lett.***2004**, *85*, 739.
DOI: [10.1063/1.1776310](https://doi.org/10.1063/1.1776310)
34. Lambert, S.; Leligny, H.; Grebille, D.; *J. Solid State Chem.***2001**, *160*, 322.
DOI: [10.1006/jssc.2001.9235](https://doi.org/10.1006/jssc.2001.9235)
35. Grebille, D.; Lambert, S.; Bourée, F.; Petricek, V.; *J. Appl. Cryst.***2004**, *37*, 823.
DOI: [10.1107/S0021889804018096](https://doi.org/10.1107/S0021889804018096)
36. Wu, L.; Meng, Q.; Jooss, C.; Zheng, J. C.; Inada, H.; Su, D.; Li, Q.; Zhu, Y.; *Adv. Funct. Mater.***2013**, *23*, 5728.
DOI: [10.1002/adfm.201301098](https://doi.org/10.1002/adfm.201301098)
37. Lotgering, F. K.; *J. Inorg. Nucl. Chem.***1959**, *9*, 113.
DOI: [10.1016/0022-1902\(59\)80070-1](https://doi.org/10.1016/0022-1902(59)80070-1)
38. Xu, G.; Funahashi, R.; Shikano, M.; Matsubara, I.; Zhou, Y.; *Appl. Phys. Lett.***2002**, *80*, 3760.
DOI: [10.1063/1.1480115](https://doi.org/10.1063/1.1480115)
39. Sugiyama, J.; Brewer, J. H.; Ansaldo, E. J.; Itahara, H.; Dohmae, K.; Seno, Y.; Xia, C.; Tani, T.; *Phys. Rev. B.***2003**, *68*, 134423.
DOI: [10.1103/PhysRevB.68.134423](https://doi.org/10.1103/PhysRevB.68.134423)
40. Sugiyama, J.; Itahara, H.; Tani, T.; Brewer, J. H.; Ansaldo, E. J.; *Phys. Rev. B.***2002**, *66*, 134413.
DOI: [10.1103/PhysRevB.66.134413](https://doi.org/10.1103/PhysRevB.66.134413)
41. Wu, T.; Tyson, T. A.; Chen, H.; Bai, J.; Wang, H.; Jaye, C.; *J. Phys. Condens. Matter.***2012**, *24*, 455602.
DOI: [10.1088/0953-8984/24/45/455602](https://doi.org/10.1088/0953-8984/24/45/455602)
42. Guilmeau, E.; Funahashi, R.; Mikami, M.; Chong, K.; Chateigner, D.; *Appl. Phys. Lett.***2004**, *85*, 1490.
DOI: [10.1063/1.1785286](https://doi.org/10.1063/1.1785286)
43. Chaikin, P. M.; Beni, G.; *Phys. Rev. B***1976**, *13*, 647.
DOI: [10.1103/PhysRevB.13.647](https://doi.org/10.1103/PhysRevB.13.647)
44. Mizokawa, T.; Tjeng, L. H.; Lin, H. J.; Chen, C. T.; Kitawaki, R.; Terasaki, I.; Lambert, S.; Michel, C.; *Phys. Rev. B.***2005**, *71*, 193107.
DOI: [10.1103/PhysRevB.71.193107](https://doi.org/10.1103/PhysRevB.71.193107)
45. Mikami, M.; Guilmeau, E.; Funahashi, R.; Chong, K.; Chateigner, D.; *J. Mater. Res.***2005**, *20*, 2491.
DOI: [10.1557/jmr.2005.0298](https://doi.org/10.1557/jmr.2005.0298)